6-6-2016

Motion of the MMS Spacecraft Relative to the Magnetic Reconnection Structure Observed on 16 Oct 2015 at 1307 UT

Richard Denton
Dartmouth College

O. Sonnerup
Dartmouth College

H. Hasegawa
Institute of Space and Astronautical Science, JAXA, Sagamihara, Japan

D. Phan
University of California - Berkeley

C.T. Russell
University of California, Los Angeles

See next page for additional authors

Motion of the MMS Spacecraft Relative to the Magnetic Reconnection Structure Observed on 16 Oct 2015 at 1307 UT

R. E. Denton[1], B.U.Ö. Sonnerup[2], H. Hasegawa[3], T. D. Phan[4],

C. T. Russell[5], R. J. Strangeway[5], B. L. Giles[6], D. Gershman[6,7], and

R. B. Torbert[8]

Abstract. We analyze a magnetopause crossing by the Magnetospheric Multiscale (MMS) spacecraft at 1307 UT on 16 Oct 2016 that showed features of electron scale reconnection. For this event, we find orthonormal LMN coordinates from the magnetic field, with N and L varying respectively along the maximum gradient and maximum variance directions. We find the mo-

---

R. E. Denton, 32 Oak Tree Dr., New Smyrna Beach, FL 32169, USA. (redenton@dartmouth.edu)

D. Gershman, (daniel.j.gershman@nasa.gov)

B. L. Giles, Mail Code 673, Building 21, Room 063, Goddard Space Flight Center, Greenbelt MD 20771, USA. (barbara.giles@nasa.gov)

H. Hasegawa, Institute of Space and Astronautical Science, JAXA, Yoshinodai 3-1-1, Chuo-ku, Sagamihara, Kanagawa, 252-5210, Japan. (hase@stp.isas.jaxa.jp)

T. D. Phan, Space Sciences Laboratory, UC Berkeley, 7 Gauss Way, Berkeley, CA 94720, USA. (phan@ssl.berkeley.edu)

C. T. Russell, and R. J. Strangeway, Institute of Geophysics and Planetary Physics, UCLA, Los Angeles, CA 90024-1567, USA. (ctrussel@igpp.ucla.edu,strange@igpp.ucla.edu)

B.U.Ö Sonnerup, Thayer School of Engineering, Dartmouth College, Hanover, NH 03755, USA. (bengt.u.o.sonnerup@dartmouth.edu)

R. B. Torbert, Institute for the Study of Earth, Oceans, and Space, Morse Hall, UNH, 8 College Road, Durham, NH 03824-3525, USA. (Roy.Torbert@unh.edu)

[1]Department of Physics and Astronomy,

tion along N from the Spatio-Temporal Difference analysis and motion along L from measured particle velocities. We locate the position of the magnetic X point, finding that MMS-4 passed within about 1.4 km from the X point and that MMS-3 and MMS-2 passed within about 1.7 km and 2.4 km, respectively, from the position of maximum out of plane current.

Dartmouth College, Hanover, New

Hampshire, USA

[2]Thayer School of Engineering, Dartmouth College, Hanover, New Hampshire, USA

[3]Institute of Space and Astronautical Science, JAXA, Sagamihara, Japan.

[4]Space Science Laboratory, University of California at Berkeley, Berkeley, California, USA.

[5]Institute of Geophysics and Planetary Physics, University of California at Los Angeles, Los Angeles, California, USA.

[6]NASA Goddard Space Flight Center, Greenbelt, MD, USA.

[7]Department of Astronomy, University of Maryland, College Park, Maryland, USA.

[8]Institute for the Study of Earth, Oceans, and Space, University of New Hampshire, Durham, New Hampshire, USA.

1. Introduction

The primary goal of NASA's Magnetospheric Multiscale (MMS) mission is to investigate the kinetic processes occurring in the small-scale region called the electron diffusion region [*Hesse et al.*, 2014; *Burch et al.*, 2015]. In this region neither particle species is "frozen-in" or carried along with magnetic flux in directions perpendicular to the magnetic field **B**. Recently the MMS Science Working Team has identified an event observed by the MMS spacecraft at 16 Oct 2015, 1307 UT, as possibly probing this region [*Burch et al.*, 2016].

Our purpose here is to identify for this event the directions that describe the reconnecting magnetic structure, the velocity of that structure relative to the spacecraft, and the paths of the spacecraft relative to that structure. We define the X point as the position where the magnetic field reverses in direction and away from which the reconnected plasma is ejected.

Methods to determine the orientation and velocity from single spacecraft data have been described by *Sonnerup and Scheible* [1998], *Khrabrov and Sonnerup* [1998], *Sonnerup et al.* [2013], and references therein. Methods using multi spacecraft data have been described by *Schwartz* [1998], *Dunlop and Woodward* [1998], *Shi et al.* [2005], *Shi et al.* [2006], *Denton et al.* [2012], and references therein.

2. Event and Data

On 16 Oct 2015 at 1307 UT, the four MMS spacecraft were at X, Y, and Z Geocentric Solar Magnetospheric (GSM) coordinates of 8.30, 7.05, and -4.82, respectively, in units of the Earth's radius, R_{E}. The spacecraft were in an approximately symmetric tetrahedral configuration with a nominal separation of 10 km.

Using asymptotic values for the magnetosphere and magnetosheath from the Movie 1 caption of *Burch et al.* [2016] and formulas by *Cassak and Shay* [2007], we find the outflow speed $V_{\rm out,CS} = 241$ km/s and the hybrid density $n_{\rm out,CS} = 7.4$ cm^{-3}, from which we find the ion inertial length, $\delta_{\rm ion} = 84$ km. (The Cassak and Shay formulas do not include a guide field [out of reconnection plane]; a small guide field seems to be present for this event [section 5].)

We used burst mode FluxGate Magnetometer (FGM) data [*Russell et al.*, 2014]. The data with a resolution of 0.0078 s were boxcar averaged every five data points yielding a resolution of 0.039 s.

We used burst mode ion and electron bulk velocity moments from the Fast Plasma Instrument (FPI) [*Pollock et al.*, 2016]. The resolution of the electron moments was 30 ms, and that of the ions (measured collectively) was 150 ms. We verified that ion density was within about 10% of the electron density at the resolution of the ion instrument.

3. Orientation of the Reconnecting Structure

We define an orthogonal "LMN" coordinate system with $\mathbf{e}_L$ along the reconnection magnetic field roughly northward, $\mathbf{e}_N$ across the current sheet roughly outward, and $\mathbf{e}_M$ roughly westward. Figure 1c shows the magnetic field averaged over the four spacecraft, $\mathbf{B}_{\rm av}$, for a period of five seconds using the LMN coordinates described below. In this paper, time t will always indicate seconds following 1307 UT.

To get the L direction, we found the direction of maximum variance of the magnetic field [*Sonnerup and Scheible*, 1998], collecting the data from all four spacecraft. Concentrating on the current sheet crossing, we used the time interval 2.3 ± 0.5 s to find $\mathbf{e}_L =$ (0.311,0.488,0.816) in GSM. The statistical uncertainty using equation 8.23 of *Sonnerup*

and Scheible [1998] is 2.3°. Using time intervals up to a factor of 4 larger yielded variation in the direction of less than 3°, suggesting that the statistical error is reasonable.

To get the N direction, we used the technique of *Shi et al.* [2005], that they call Minimum Directional Derivative analysis. This method computes a matrix from the gradient of the vector magnetic field calculated using the field and positions of the four spacecraft, $\partial_i B_j$, then multiplies this matrix by its transpose to form a symmetric matrix. This second matrix is diagonalized to find the eigenvalues and eigenvectors associated with the gradient. We get $\mathbf{e}_N$ from the maximum gradient direction that is across the current sheet. Results were similar using the modified method with the perturbed gradient as described by *Denton et al.* [2010, 2012].

It was necessary to use both of these methods to define the LMN coordinate system for this time interval because the intermediate and minimum eigenvalues for both methods were not well separated (factor of 5.1 for the magnetic variance and factor of 1.7 for the Shi method matrix), indicating a poor determination of the other directions.

The eigenvalues from the Shi et al. method are shown in Figure 1a. Separation of the maximum eigenvalue (black curve in Figure 1a) from the other eigenvalues (blue and red curves in Figure 1a) was good for much of the time interval plotted. To get $\mathbf{e}_N$, we used the maximum gradient direction $\mathbf{e}_{\mathrm{G,max}}$ in the same time interval, 2.3 ± 0.5 s. The vector $\mathbf{e}_{\mathrm{G,max}}$ is time dependent and defines a time varying direction $\mathbf{e}_{N'}$ (Figure 1b). To obtain a single N direction, we averaged the squared gradient matrix [*Denton et al.*, 2010, 2012] to find the maximum gradient eigenvector (0.803,0.274,.-0.529), plotted as the asterisks in Figure 1b. This direction is 92.7° from $\mathbf{e}_L$ determined above. The standard deviation $\mathbf{e}_{N'}$ away from the average direction was 17.5°, but the uncertainty of the mean (dividing

by $\sqrt{N-1}$) was only 3.5°. Subtracting off the component of the vector parallel to $\mathbf{e}_L$ and re-normalizing, we found $\mathbf{e}_N$ = (0.819,0.296,-0.490), plotted as the open circles in Figure 1b. Then $\mathbf{e}_M = \mathbf{e}_N \times \mathbf{e}_L$ = (0.480,-0.820,0.307). The $\mathbf{e}_N$ direction is 14° off from the normal from the *Shue et al.* [1998] magnetopause model. Note that we could have equally well used $\mathbf{e}_N$ without adjustment, and adjusted $\mathbf{e}_L$; or we could have made some intermediate choice.

Close to the current sheet, the minimum gradient direction, which was erratic, tended to be more aligned with our maximum variance direction L than with our M direction. This indicates that the structure probably had significant variation in all three directions. Nevertheless we will describe the average two dimensional structure in what we call the reconnection plane that includes L and N.

In Figure 1c, the L component of $\mathbf{B}_{\rm av}$, $B_{{\rm av},L}$, was largest and positive for $t < 2.3$ s, indicating that the spacecraft crossed from the magnetosphere into the magnetosheath. The oscillations in $B_{{\rm av},L}$ may indicate non-monotonic motion.

4. Motion of the Magnetic Structure

The *Shi et al.* [2006] method, that they call "Spatio-Temporal Difference" analysis, can be used to get the velocity of the magnetic structure relative to the average position of the spacecraft, $\mathbf{V}_{\rm str} = -\mathbf{V}_{\rm sc}$, where $\mathbf{V}_{\rm sc}$ is the velocity of the spacecraft relative to the structure. At each moment in time, the structure is assumed to be time invariant and moving with constant velocity so that the observed rate of change of $\mathbf{B}$ is $\mathrm{d}\mathbf{B}/\mathrm{d}t = \mathbf{V}_{\rm sc}\cdot\nabla\mathbf{B}$. Given that $\nabla\mathbf{B}$ is known from the *Shi et al.* [2005] method discussed in section 3, this equation can be inverted to yield $\mathbf{V}_{\rm sc}$ versus time from the observed $\mathrm{d}\mathbf{B}_{\rm av}/\mathrm{d}t$.

Since the inversion schematically divides $d\mathbf{B}/dt$ by the gradient of $\mathbf{B}$, the resulting values of $\mathbf{V}_{str} = -\mathbf{V}_{sc}$ will have large errors in the directions for which $\nabla\mathbf{B}$ is small. Typically the component in the direction of the minimum gradient eigenvector from the *Shi et al.* [2005] method is greatly in error [*Denton et al.*, 2010, 2012]. For our event, the intermediate gradient component may also at times be unreliable. In Figure 2b, we show $V_{str,N}$, the N component of $\mathbf{V}_{str}$, calculated in three different ways. The gold curve uses the full vector velocity constructed from all three components of the point by point $\mathbf{V}_{str}$, the green curve uses only the point by point maximum and intermediate gradient directions, and the blue curve uses only the point by point maximum gradient direction. In each case, the velocity constructed from these components is dotted into $\mathbf{e}_N$.

The gold, green, and blue curves in Figure 2c show the time integral of the corresponding velocity components plotted in Figure 2b, yielding the displacement of the structure relative to the spacecraft in the N direction, dN_{str}. All three curves are very consistent between about $t = 1.8$ s and 2.7 s. This region includes $t \sim 2.3$ s, the time of steepest gradient in $B_{av,L}$ (Figure 2a), the magnetic reversal ($B_{av,L} = 0$), marked by the vertical gray dotted lines in Figure 2a–c, and the flow reversal in the L direction, as we will show below. Therefore this region will turn out to be the crucial region for determining the position of the X point.

Outside of this interval, we do not know, a priori, which calculation of dN_{str} is more accurate. Potentially, the gold curve in Figure 2c, having been calculated using all three components of the point by point $\mathbf{V}_{str}$, could contain the most information. The gold curve in Figures 2b and 2c is fairly well behaved between $t = 1.77$ s and 3.49 s. But the large off scale oscillations for the gold curve outside of that interval suggest that it

is unreliable at those times. Note that if the magnetic structure moves outward, then the spacecraft will be moving into the magnetosphere where B is larger. So if the time variation of $B_{\mathrm{av},L}$ in Figure 2a results mainly from motion normal to the current sheet (across a gradient in $B_{\mathrm{av},L}$), then the time dependence of the displacement in Figure 2c ought to look similar to the time dependence of $B_{\mathrm{av},L}$ in Figure 2a. Both the green and blue curves in Figure 2c show some similarity to $B_{\mathrm{av},L}$.

For reasons that we will be easier able to explain later, we use, for the purposes of calculating the spacecraft motion, the average of the gold curve and blue curve in Figure 2b for $\mathbf{V}_{\mathrm{str},N}$ for $t = 1.77$ s to 3.49 s, and the average of the green and blue curve in Figure 2b for $\mathbf{V}_{\mathrm{str},N}$ outside of that time interval. (A rough estimate of the gradient due to fluctuations at the precision of the magnetometers suggests that the gold curve could possibly be accurate in most of the region $t = 1.77$ s to 3.49 s.) This procedure is a compromise in each region, inner and outer, between the potentially more accurate velocity and the safer velocity from the maximum gradient direction alone. The displacement calculated using this hybrid velocity leads to the gray dashed curve in Figure 2c. Using this curve for the displacement leads to better agreement with the observations, as we will discuss in section 5.

For reasons not understood, the electron and ion velocities along our N direction (not shown) have large opposite flow during the time interval from $t = 0$ to the vertical dotted line in Figure 2a–c, with the electrons moving outward (positive N direction) and the ions moving inward. If, instead, we dot the electron and ion velocities with the instantaneous normal directions, $\mathbf{e}_{N'}$, and integrate that velocity to find a normal displacement, both the electrons and ions oscillate in and out in a manner similar to the motion in Figure 2c, but

with different velocities. The electron velocity is the largest, and the magnetic structure has a normal velocity intermediate between the electron and ion velocities.

As a check of our values of $V_{\mathrm{str},N}$, we used the timing analysis described by *Schwartz* [1998]. In Figure 3a, we show B_L for the four MMS spacecraft (solid curves) and the same data smoothed with a running average over 5 data points (dotted curves). Using spacecraft positions at the times of maximum gradient (circles in Figure 3a), we found the normal direction and velocity of a plane crossing the spacecraft. This normal direction was (0.692,0.431,-0.579), which is 12.1° from our more accurate N direction. The normal velocity from the timing analysis was -43. km/s (red dot in Figure 2b; *Burch et al.* [2016] found -45 km/s), 10% off from the average of the gold and blue curves in Figure 2b at that time (-48 km/s).

Figure 3b shows the L component of the electron velocity, $V_{\mathrm{e},L}$, for the four MMS spacecraft, and Figure 3c shows the average L component of the electron velocity, $V_{\mathrm{e,av},L}$ (green curve) and ion velocity, $V_{\mathrm{ion,av},L}$ (blue curve). There is a lot of spatial structure in the electron velocity leading to the differences between the curves for the different spacecraft in Figure 3b, but $V_{\mathrm{e,av},L}$ (green curve in Figure 3c) exhibits a clear linear ramp between $t = 2.03$ s and 2.47 s, marked off by the two vertical dotted lines in Figure 3c. At the midpoint of this ramp, $t = 2.25$ s, the blue curve for $V_{\mathrm{ion,av},L}$ crosses the green curve for $V_{\mathrm{e,av},L}$. We infer that the centroid of the spacecraft passed the X point in the L direction at that time, and that the common velocity at that time, -97 km/s, is the L component of the velocity of the reconnection structure. Both $V_{\mathrm{e,av},L}$ and $V_{\mathrm{ion,av},L}$ are more negative than that velocity for $t < 2.25$ s and more positive for $t > 2.25$ s. So both the electrons and ions are flowing outward in the L direction away from the X point. Since

the L direction is northward and the spacecraft are at negative Z, this means that the X point is moving away from the magnetic equator. Relative to the X point, the plasma is flowing away from the magnetic equator for $t < 2.25$ s, and toward the magnetic equator for $t > 2.25$ s. Based on the 97 km/s structure velocity, the end of the linear ramp in Figure 3c is 0.25 $\delta_{\rm ion}$ downstream.

The green and blue curves in Figure 2d are respectively $V_{\rm e,av,L}$ and $V_{\rm ion,av,L}$ shifted up by 97 km/s for a longer time interval, t = -5 s to 8 s. The vertical solid line is at $t = 2.25$ s, where the electron and ion L velocities diverge from zero, and the adjacent vertical dotted lines are drawn at the limits of the linear ramp in $V_{\rm e,av,L}$ from Figure 3c; the ion velocity also has a roughly linear ramp between the more separated vertical dashed lines. Moving to the left in Figure 2d from the flow reversal at 2.25 s, the ion velocity is smaller than the electron velocity until the end of the ion velocity ramp 7.2 $\delta_{\rm ion}$ downstream. The electron velocity and the ion velocity on the left side of Figure 2d accelerate to an outflow speed matching $V_{\rm out,CS}$, the Cassak-Shay outflow jet speed (horizontal dotted lines in Figure 2d).

5. Paths of the Spacecraft Relative to the Reconnection Structure

We have assumed that the reconnection structure is moving in the L direction with the common velocity -97 km/s of the electrons and ions (Figure 3c) at $t = 2.25$ s. The roughly linear variation of $V_{\rm ion,av,L}$ (Figure 2d) indicates that the L component of the structure velocity does not vary greatly in an interval around $t = 2.25$ s. For the purpose of visualizing the spacecraft paths, we assume that this velocity is constant.

In Figure 4c the black arrows, short magenta arrows, and long magenta arrows show respectively the directions of the reconnection magnetic field B_L, the plasma inflow velocity $V_{\rm in}$, and the plasma outflow velocity $V_{\rm out}$. The thick gold curve in Figure 4c is the

trajectory of the centroid of the MMS spacecraft ("MMS-Av") relative to the magnetic structure in the L-N plane. The displacement in the N direction, $N_{\rm sc,Shi}$, is the negative of the gray dashed curve for $\mathrm{d}N_{\rm str}$ in Figure 2c, defined so it is zero at the magnetic reversal at $t = 2.47$ s. The displacement in the L direction is $L_{\rm sc,97km/s} = (t - 2.25\ \mathrm{s})(97\ \mathrm{km/s})$, so that it is zero at the flow reversal at $t = 2.25$ s. So the origin is where we estimate the X point to be. Based on the gold curve in Figure 4c, the spacecraft oscillated toward and away from the current sheet, crossed $L = 0$ (flow reversal), crossed $N = 0$ (magnetic reversal), wandered in the L direction, and then crossed back over $N = 0$ near $t = 5$ s.

Figure 4c also shows the trajectories of the individual MMS spacecraft using the colors indicated in the legend. These trajectories are displaced from the trajectory of the centroid by the relative displacement of each spacecraft (see starting point of curves).

Figure 4a shows B_L averaged over the four spacecraft ("MMS-Av") and for the individual spacecraft, versus the time t_{Av}. This time is equivalent to t only for MMS-Av. The other curves have been shifted horizontally so that the observed field components line up vertically with the corresponding position in panel c (see starting point of curves). The oscillations in $N_{\rm sc,Shi}$ to the left of the vertical line in Figure 4c are strongly correlated with the oscillations in B_L in Figure 4a. Generally the lowest B_L values in Figure 4a occur for the spacecraft with the largest $N_{\rm sc,Shi}$ values. The MMS-2, MMS-3, and MMS-4 spacecraft passed quickly through the magnetic reversal at $N_{\rm sc,Shi} = 0$, and correspondingly B_L in Figure 4a reversed quickly for these spacecraft. But the motion in the N direction stagnated when MMS-1 was near the magnetic reversal ($L_{\rm sc,97km/s} \sim 75$ km in Figure 4c). Correspondingly, MMS-1 observed B_L near zero at that time (Figure 4a).

The L and N axes in Figure 4c divide space into four quadrants. For symmetric (same conditions in magnetosphere and magnetosheath) anti-parallel (no guide field) reconnection, the sign of B_M should be positive into the page in the bottom left and upper right quadrants of Figure 4c [e.g., Figure 5c of *Sonnerup et al.*, 2016], as indicated by the green arrow heads pointing into the page in Figure 4c. Then B_M would be negative out of the page in the upper left and bottom right quadrants of Figure 4c. For asymmetric reconnection, this quadrapolar structure is not necessarily expected [*Mozer et al.*, 2008], but the structure of B_M does appear to be quadrapolar for this event. Note that during the time that MMS-Av crossed into the lower right quadrant (just to the right of the origin in Figure 4c), the average B_M is negative. According to Figure 4c, MMS-1 penetrated most deeply (near $L_{\mathrm{sc,97km/s}} = 0$) into the lower right quadrant. Correspondingly, B_M became most negative for MMS-1. MMS-1 penetrated the least into the magnetosheath (upper region in Figure 4c), and correspondingly, B_M became least positive for MMS-1 on the right side of Figure 4b. When MMS-4 was near the X point (the origin in Figure 4c), it observed a minimum in B_M, ~ -2.5 nT. This suggests that there was a small guide field of about 1/10 of the asymptotic magnetosheath field.

According to Figure 4, MMS-4 passed nearest to the X point, within 1.3 km on the lower right side of the X point in Figure 4 at $t = 2.35$ s. Supplementary Figure S1 shows that MMS-4 measured a minimum in the total magnetic field B or the magnetic field calculated from the L and N components (allowing for the possibility of a guide field), B_{LN}, between about $t = 2.3$ s and 2.33 s.

According to *Burch et al.* [2016], the electron dissipation region where the electron kinetic effects were most important was not at the magnetic reversal, but at the peak in

the M component of the plasma current, J_M. We calculated the average current density using FPI data, and found that this peaked at $t = 2.20$ s. The position of MMS-Av at this time is marked by the intersection of the thick gold curve with the horizontal dotted line in Figure 4. We assume that the intersection of this line with the flow reversal is where the greatest amount of dissipation occurred. According to our model, MMS-2 and MMS-3 had the closest approach to this intersection, with MMS-3 coming within 1.7 km at $t = 2.19$ s and MMS-2 within 2.4 km at $t = 2.21$ s. According to our calculations using the FPI data, MMS-3 observed the largest negative J_M, -11,800 e cm^{-3} km/s (where e is the proton charge) at $t = 2.22$ s, and MMS-2 observed the second largest negative value, -10,800 e cm^{-3} km/s at $t = 2.19$ s, followed by MMS-4 with -10,500 e cm^{-3} km/s at $t = 2.14$ s and MMS-1 with -8,200 e cm^{-3} km/s at $t = 2.55$ s.

We are not claiming that the trajectories in Figure 4 are exact. For instance, if we used the green curve in Figure 2c rather than the gray dashed curve to get $N_{\mathrm{sc,Shi}}$ in Figure 4c, we would find that MMS-4 passed within 1.9 km of the X point on the upper left side, rather than the lower right side, of the X point in Figure 4. But Figure 4c probably does correctly indicate that MMS-4 had the closest approach to the X point and that MMS-2 and MMS-3 had the closest approaches to the point where J_M peaks and the flow reverses.

We are most confident about the motion between $t = 1.8$ s and 2.7 s, during which all the curves in Figure 2c agree; the positions at the limits of this interval are marked by gold filled circles on the thick gold curve in Figure 4c. The reason that we defined the hybrid velocity leading to the gray dashed curve in Figure 2c is because use of the gray dashed curve led to better agreement with the observations outside of the gold filled circles in Figure 4c. Using the gray dashed curve, the trajectory of MMS-1 (black curve

in Figure 4c) is very close to $N = 0$ when B_L for MMS-1 is close to zero (black curve in Figure 4a) and the magnetic field observed by MMS-1 is at a minimum (black curve in Figure S1e). If we had used the gold curve alone in the central region, MMS-1 would have gone more deeply into the magnetosheath, whereas if we had used the blue curve alone in the central region, MMS-1 would have stayed more deeply in the magnetosphere. If we had used the blue curve alone for the outer region, MMS-4 would have oscillated across the magnetic reversal ($N = 0$) at early times, whereas B_L in Figure 4a suggests that MMS-4 stayed within the magnetosphere during the oscillations. Or if we had used the green curve alone for the outer region, MMS would not have returned into the magnetosphere near $t_{Av} = 4.7$ s as suggested by B_L in Figure 4a.

Though there is evidence of significant spacecraft dependent structure in the M direction, we have nevertheless found a good description of the average structure in the reconnection plane including the reconnection magnetic field and the direction across the current sheet at 1307 UT. By using the data from multiple spacecraft, we have been able to determine the orientation of the magnetic structure, the velocity of the magnetic structure in the L-N plane, and the paths of the spacecraft relative to that structure.

Acknowledgments. Work at Dartmouth was supported by NASA grant NNX14AC38G. H. H. was supported by JSPS Grant-in-Aid for Scientific Research KAKENHI 15K05306. Solar wind parameters and geomagnetic indices were obtained from the GSFC/SPDF OMNIWeb interface at http://omniweb.gsfc.nasa.gov. R. D. thanks Mike Shay, Marc Swisdak, Love Alm, and Paul Cassak for useful discussions. B. G. thanks Levon Avanov and John Dorelli for help in advancing the quality of the FPI products. MMS data are available at https://lasp.colorado.edu/mms/sdc/public/links. Supplementary data from

our calculations can be found in the Supplementary Information file. In addition to Supplementary Figure S1 referenced in the text, Supplementary Text S1 to S3 has more detail on the calculation of the LMN coordinate system. Supplementary Dataset S1 lists the velocities and directions from the *Shi et al.* [2005, 2006] method, while Dataset S2 lists the L and N positions that we calculated.

References

Burch, J. L., T. E. Moore, R. B. Torbert, and B. L. Giles (2015), Magnetospheric Multiscale Overview and Science Objectives, *Space Science Reviews*, doi:10.1007/s11214-015-0164-9.

Burch, J. L., et al. (2016), Electron-scale measurements of magnetic reconnection in space, *Science*, in press.

Cassak, P. A., and M. A. Shay (2007), Scaling of asymmetric magnetic reconnection: General theory and collisional simulations, *Phys. Plasmas*, *14*, 102114, doi:10.1063/1.2795630.

Denton, R. E., B. U. O. Sonnerup, J. Birn, W. L. Teh, J. F. Drake, M. Swisdak, M. Hesse, and W. Baumjohann (2010), Test of methods to infer the magnetic reconnection geometry from spacecraft data, *J. Geophys. Res.*, *115*, a10242, doi:10.1029/2010ja015420.

Denton, R. E., B. U. O. Sonnerup, M. Swisdak, J. Birn, J. F. Drake, and M. Hesse (2012), Test of Shi et al. method to infer the magnetic reconnection geometry from spacecraft data: MHD simulation with guide field and antiparallel kinetic simulation, *J. Geophys. Res.*, *117*, a09201, doi:10.1029/2012ja017877.

Dunlop, M. W., and T. I. Woodward (1998), Multi-spacecraft discontinuity analysis: Orientation and motion, in *Analysis Methods for Multi-Spacecraft Data*, edited by G. Paschmann and P. Daly, pp. 271–306, International Space Science Institute, SR-001, Bern Switzerland.

Hesse, M., et al. (2014), Theory and modeling for the Magnetospheric Multiscale Mission, *Space Science Reviews*, doi:10.1007/s11214-014-0078-y.

Khrabrov, A. V., and B. U. O. Sonnerup (1998), DeHoffmann-Teller Analysis, in *Analysis Methods for Multi-Spacecraft Data*, edited by G. Paschmann and P. Daly, pp. 221–248, International Space Science Institute, SR-001, Bern Switzerland.

Mozer, F.S., P.L. Pritchett, J. Bonnell, D. Sundkvist, and M.T. Chang (2008), Observations and simulations of asymmetric magnetic field reconnection, *J. Geophys. Res.*, 113A00C03, doi:10.1029/2008ja013535.

Pollock, C., et al. (2016), Fast Plasma Investigation for Magnetospheric Multiscale, *Space Science Reviews*, doi:10.1007/s11214-016-0245-4.

Russell, C. T., et al. (2014), The Magnetospheric Multiscale Magnetometers, *Space Science Reviews*, doi:10.1007/s11214-014-0057-3.

Schwartz, S. J. (1998), Shock and discontinuity normals, mach numbers, and related parameters, in *Analysis Methods for Multi-Spacecraft Data*, edited by G. Paschmann and P. Daly, pp. 249–270, International Space Science Institute, SR-001, Bern Switzerland.

Shi, Q. Q., C. Shen, Z. Y. Pu, M. W. Dunlop, Q. G. Zong, H. Zhang, C. J. Xiao, Z. X. Liu, and A. Balogh (2005), Dimensional analysis of observed structures using multipoint magnetic field measurements: Application to Cluster, *Geophys. Res. Lett.*, *32*(12), l12105, doi:10.1029/2005gl022454.

Shi, Q. Q., C. Shen, M. W. Dunlop, Z. Y. Pu, Q. G. Zong, Z. X. Liu, E. Lucek, and A. Balogh (2006), Motion of observed structures calculated from multi-point magnetic field measurements: Application to Cluster, *Geophys. Res. Lett.*, *33*(8), l08109, doi: 10.1029/2005gl025073.

Shue, J. H., et al. (1998), Magnetopause location under extreme solar wind conditions, *J. Geophys. Res.*, *103*(A8), 17,691.

Sonnerup, B., and M. Scheible (1998), Minimum and maximum variance analysis, in *Analysis Methods for Multi-Spacecraft Data*, edited by G. Paschmann and P. Daly, pp. 185–220, International Space Science Institute, SR-001, Bern Switzerland.

Sonnerup, B. U. O., R. E. Denton, H. Hasegawa, and M. Swisdak (2013), Axis and velocity determination for quasi two-dimensional plasma/field structures from Faraday's law: A second look, *J. Geophys. Res.*, *118*(5), 2073–2086, doi:10.1002/jgra.50211.

Sonnerup, B. U. O., H. Hasegawa, R. E. Denton, and T. K. M. Nakamura (2016), Reconstruction of the electron diffusion region, *J. Geophys. Res.*, *121*, doi:in press.

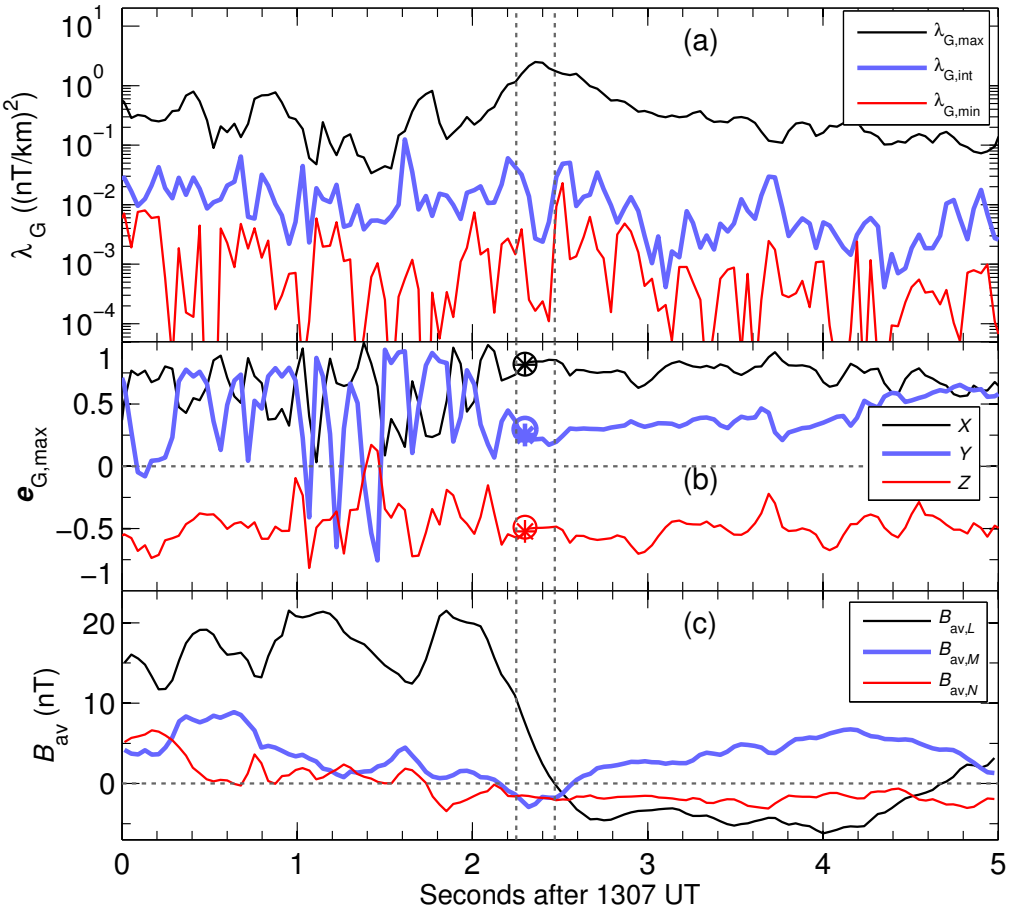

Figure 1. Results from Shi et al. method versus time: (a) Squared gradient eigenvalues λ_G. (b) GSM X, Y, and Z components of the maximum gradient eigenvector, $\mathbf{e}_{G,max}$. The asterisks and circles show, respectively, components of $\mathbf{e}_N$ from the average matrix before and after subtracting off the projection in the L direction. (c) $\mathbf{B}_{av}$ in the LMN coordinate system. The left and right vertical dotted lines show, respectively, the time of plasma flow reversal in the L direction and time of $B_{av,L}$ reversal.

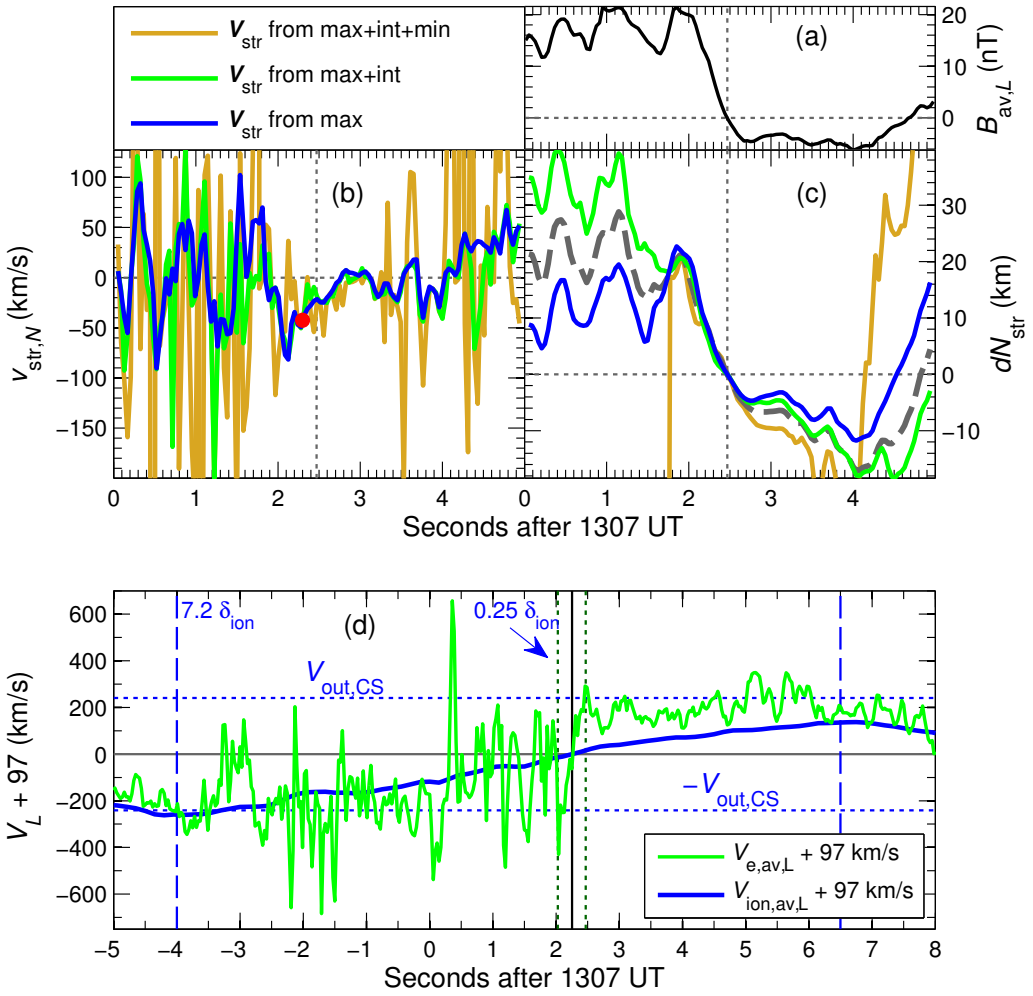

Figure 2. Structure velocities: (a) $B_{\mathrm{av},L}$ versus time. Panels (b) and (c) show, respectively, the velocity and displacement in the N direction using all three components of the point by point $\mathbf{V}_{\mathrm{str}}$ (gold curve), using only components in the maximum and intermediate gradient directions (green curve), and using only the component in the maximum gradient direction (blue curve). The red dot in panel (b) shows the result from the timing study. The gray dashed curve in panel (b) is calculated from a hybrid velocity described in the text. Panel (d) shows the average L component of the velocity shifted up by 97 km/s for electrons (green curve) and ions (blue curve). The horizontal dotted lines show the outflow speed $V_{\mathrm{out,CS}}$ and the vertical dotted and dashed lines show, respectively, the end of the electron velocity ramp at 0.25 δ_{ion} downstream and the end of the ion velocity ramp at 7.2 (at negative times) δ_{ion} downstream.

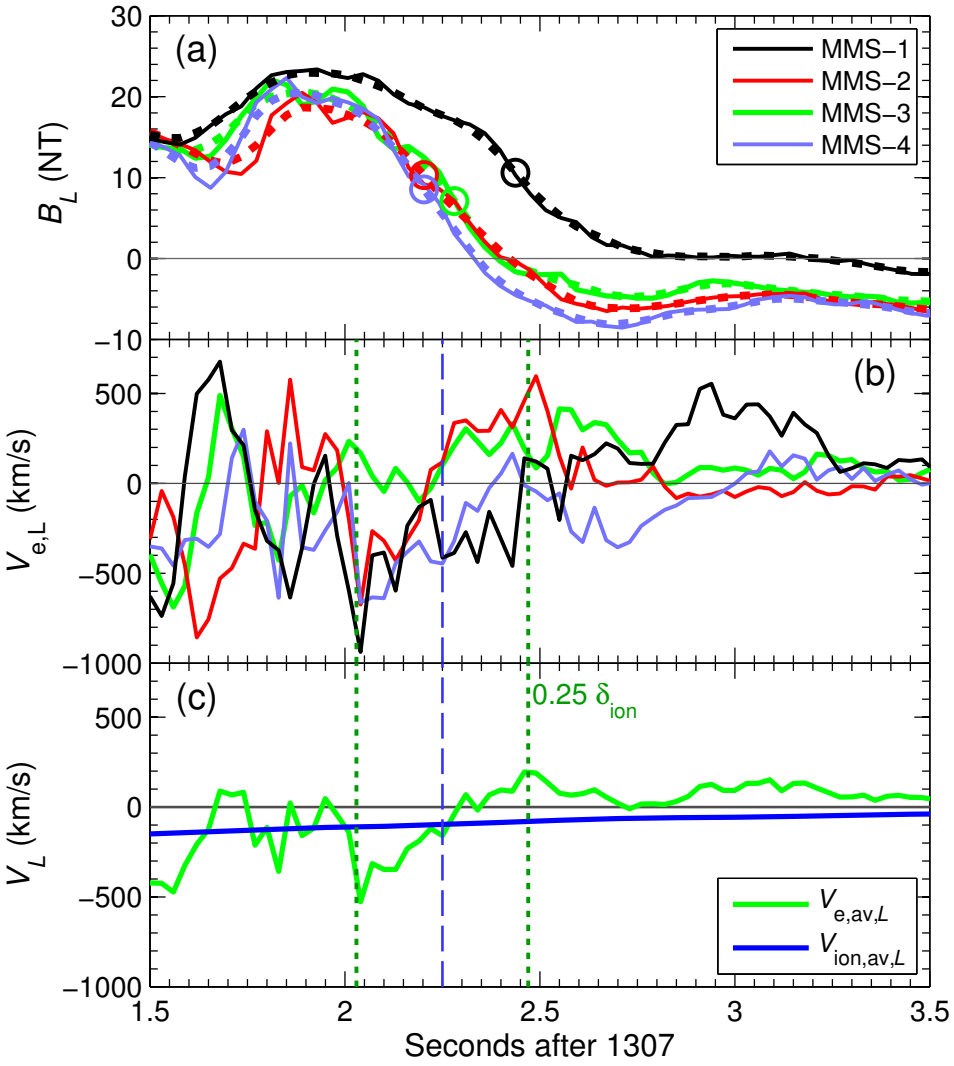

Figure 3. Behavior of L components: (a) B_L for the four MMS spacecraft (solid curves) and the same data smoothed (dotted); (b) the L component of the electron velocity, $V_{e,L}$, for the four MMS spacecraft, using the same colors as in Figure 3a; (c) the average L component of the velocity for electrons (green curve) and for ions (blue curve). The vertical dashed line is where the electron and ion velocities equal -97 km/s, and the vertical dotted lines are at the ends of the electron velocity ramp, 0.25 $\delta_{\rm ion}$ downstream (assuming 97 km/s velocity) from the location of common velocity.

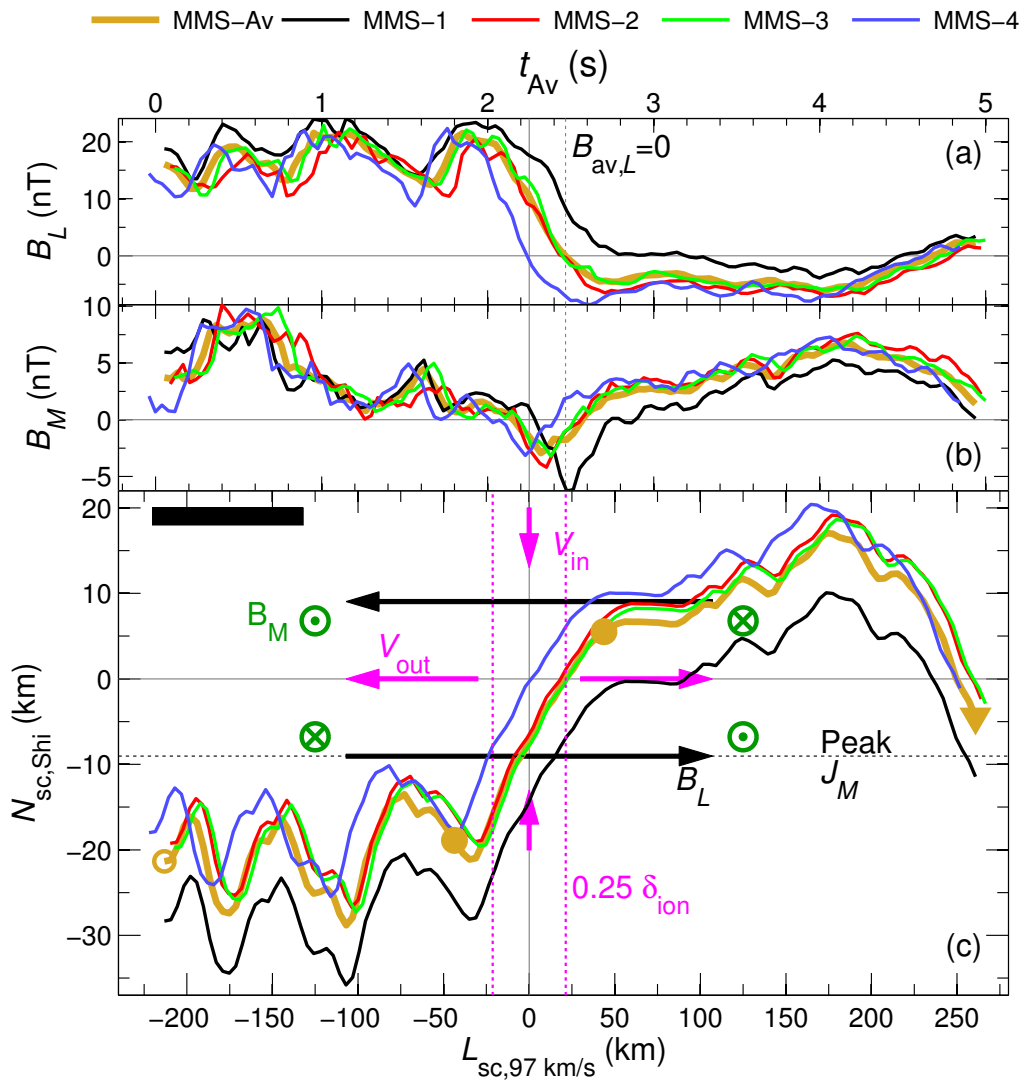

Figure 4. Spacecraft paths: (c) Trajectory of centroid ("MMS-Av") and of individual MMS spacecraft relative to the reconnection structure in the L-N plane with the X point at the origin. The centroid started at the open gold circle and ended at the downward pointing gold triangle. The gold curve is especially reliable between the gold filled circles. The filled black rectangle in the upper left corner of the panel shows the shape of the panel if the same scale for L and N were used. Panels (a) and (b) show B_L and B_M versus $t_{\rm Av}$ at the top of the plot; $t_{\rm Av}$ is the real time (following 1307 UT) only for MMS-Av. The other curves have been shifted so that the observed field components line up vertically with the corresponding position in panel c.